AD-A036 323   ROME AIR DEVELOPMENT CENTER GRIFFISS AFB N Y   F/G 17/9
MULTIPLE MODE CONTROL OF GRATING LOBES IN LIMITED SCAN ARRAYS,(U)
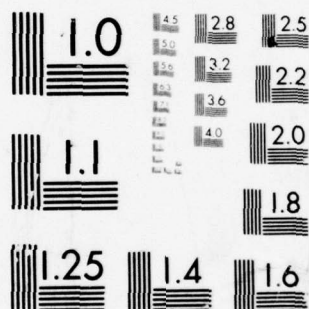SEP 76   R MAILLOUX, L ZAHN, A MARTINEZ

UNCLASSIFIED   RADC-TR-76-307   NL

| OF |
AD
A036323

END

DATE
FILMED
3-77

1.0

4.5
5.0
5.6

2.8

2.5

3.2

2.2

3.6

1.1

4.0

2.0

1.8

1.25

1.4

1.6

MICROCOPY RESOLUTION TEST CHART
NATIONAL BUREAU OF STANDARDS-1963-A

ADA036323

Multiple Mode Control of Grating Lobes in Limited Scan Arrays

ROBERT MAILLOUX
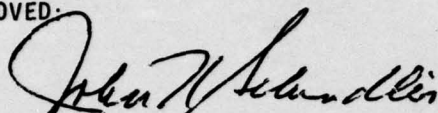LORE ZAHN
ANTHONY MARTINEZ, III, Major, USAF
GEORGE FORBES

DDC
MAR 4 1977

ROME AIR DEVELOPMENT CENTER

AIR FORCE SYSTEMS COMMAND

GRIFFISS AIR FORCE BASE, NEW YORK 13441

This report has been reviewed by the RADC Information Office (OI) and is releasable to the National Technical Service (NTIS). At NTIS it will be releasable to the general public, including foreign nations.
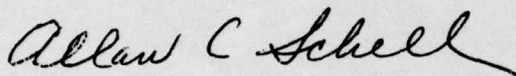
This technical report has been reviewed and approved for publication.
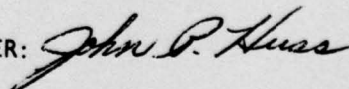
APPROVED:

JOHN K. SCHINDLER
Acting Branch Chief
Antenna and Radar Techniques Branch

APPROVED:

ALLAN C. SCHELL
Acting Chief
Electromagnetic Sciences Division

FOR THE COMMANDER:

Plans Office

REPORT DOCUMENTATION PAGE		READ INSTRUCTIONS BEFORE COMPLETING FORM
1. REPORT NUMBER RADC-TR-76-307	2. GOVT ACCESSION NO.	3. RECIPIENT'S CATALOG NUMBER
4. TITLE (and Subtitle) MULTIPLE MODE CONTROL OF GRATING LOBES IN LIMITED SCAN ARRAYS		5. TYPE OF REPORT & PERIOD COVERED In-house
		6. PERFORMING ORG. REPORT NUMBER
7. AUTHOR(s) Robert Mailloux, Lore Zahn* Anthony Martinez, III, Major, USAF George Forbes		8. CONTRACT OR GRANT NUMBER(s)
9. PERFORMING ORGANIZATION NAME AND ADDRESS Deputy for Electronic Technology (RADC) ETER Hanscom AFB Massachusetts 01731		10. PROGRAM ELEMENT, PROJECT, TASK AREA & WORK UNIT NUMBERS 62702F, 46001303
11. CONTROLLING OFFICE NAME AND ADDRESS Deputy for Electronic Technology (RADC)ETER Hanscom AFB Massachusetts 01731		12. REPORT DATE September 1976
		13. NUMBER OF PAGES 45
14. MONITORING AGENCY NAME & ADDRESS(if different from Controlling Office)		15. SECURITY CLASS. (of this report) Unclassified
		15a. DECLASSIFICATION/DOWNGRADING SCHEDULE

16. DISTRIBUTION STATEMENT (of this Report)

Approved for public release; distribution unlimited.

17. DISTRIBUTION STATEMENT (of the abstract entered in Block 20, if different from Report)

18. SUPPLEMENTARY NOTES

*Exchange scientist from the Federal Republic of Germany

19. KEY WORDS (Continue on reverse side if necessary and identify by block number)

Phased array
Antenna scanning
Array antennas

20. ABSTRACT (Continue on reverse side if necessary and identify by block number)

This report is the fourth in a series describing the use of multiple higher order modes for grating lobe control in arrays of large aperture elements scanned over restricted spatial sectors. Arrays of this type are useful in a number of applications including precision approach radar, weapons locators and satellite communications systems. The report summarizes an extensive experimental and theoretical study that includes the design and use of dielectric lenses for control of E-plane null filling for an 8-element array, the

DD FORM 1473 EDITION OF 1 NOV 65 IS OBSOLETE

309050

20.   Abstract (Continued)

investigated.   A computer model has been developed to study the effect on the boresight of a noise source in the near field of a monopulse antenna.

2

Contents

Illustrations

Tables

Multiple Mode Control of Grating Lobes in Limited Scan Arrays

1. INTRODUCTION

Limited scan antenna systems are an important and new area of phased array technology. Their importance lies in their application to air traffic control systems, fire control systems, weapons locators and communications antennas for synchronous satellites. The literature now contains references to a myriad of limited scan antenna types, *from combination of scanning reflectors to systems* based solely on array approaches, and this literature has recently been surveyed by a number of authors.[1-4] The goal of all of these systems is to minimize antenna cost by using relatively few phase controls to scan a large antenna aperture.

1. Patton, W. T. (1972) Limited scan arrays, in Phased Array Antennas, Proc. 1970 Phased Array Antenna Symposium, A. A. Oliner and G. H. Knittel, Ed., Artech House, Inc., Dedham, Mass., pp. 332-343.

2. Tang, R. (1972) Survey of time-delay beam steering techniques, in Phased Array Antennas, Proc. 1970 Phased Array Antenna Symposium, Artech House, Inc., Dedham, Mass., pp. 254-260.

3. Mailloux, R. J., and Blacksmith, P. (1974) Array and reflector techniques for airport precision approach radars, Microwave Journal, pp. 35-38.

4. Howell, J. M. (1974) Limited scan antennas, IEEE Trans. APS International Symposium.

Of all the available approaches, the array techniques are the newest and least developed. These techniques take advantage of the limited sector coverage to reduce the number of phase controls by using large elements or subarrays, and can be grouped into three categories: those consisting of overlapped or interlaced subarrays[2, 5, 6] which use narrowed and shaped subarray patterns for grating lobe suppression; those which use aperiodic element spacing to redistribute the grating lobe energy in space;[1, 8] and those in which grating lobes are suppressed by active control of the element pattern as a function of scan angle.[7]

This report summarizes the results of an extensive theoretical and experimental study program related to the use of large aperture horn elements in a limited scan array. The report presents data that addresses the potential and the limitations of the technique and includes enough background material so that this new approach can be placed in perspective.

Limited scan antenna systems can have very different forms, but some indication of relative system cost is given by a comparison of the number of active phase controls required to scan a given angular volume. Although stated in various forms by several authors,[1, 9, 10] the condition is that the minimum number of phase controls necessary to scan a given volume is equal to the number of antenna beams required to fill that volume. This condition can be made quite rigorous for orthogonal beams with uniform illumination,[9] but it has not been fully generalized to the case of low sidelobe illuminations or strained to the limits of allowing given ripple levels within the scan sector.

Nevertheless, this accounting of the minimum number of phase shifters will be used throughout this paper in the following form for maximum scan angles θ^1 max and θ^2 max in the two principal planes, and half power beamwidths θ_3^1 and θ_3^2 in these planes (with all angles expressed in radians).

5. Mailloux, R.J. (1974) An overlapped subarray for limited scan application, IEEE Trans AP AP-22:487-489.

6. Stangel, J., and Ponturieri, J. (1972) Random subarray techniques in electronic scan antenna design, IEEE G-AP International Symposium.

7. Mailloux, R.J., and Forbes, G.R. (1973) An array technique with grating-lobe suppression for limited-scan application, IEEE Trans. AP AP-21 (No. 5):597-602.

8. Manwarren, T.A., and Minuti, A.H. (1974) Zoom Feed Technique Study, RADC-TR-74-56, Final Technical Report.

9. Stangel, J.J. (1974) A basic theorem concerning the electronic scanning capabilities of antennas. Paper presented at URSI Commission VI spring meeting.

10. Borgiotti, G.V. (1975) Degrees of freedom of an antenna scanned in a limited sector, IEEE Trans AP-S International Symposium.

A reasonable minimal number of phase controls is therefore given by

$$N_{min} = 4 \ \frac{\sin \theta^1_{max} \ \sin \theta^2_{max}}{\theta^1_3 \ \theta^2_3}$$ (1)

for a rectangular scan sector and pencil or elliptical beam antennas. The ratio of the number required of phase controls to this N_{min} is therefore a measure of the economy of phase shifter usage for any given antenna and has been named the _element use factor_ by Patton.[1] In this form the equation can be applied to describe an estimate of the minimum number of phase shifters for rectangular arrays used alone or as a feed for scanned reflector or lens systems. In principle, the formula should be modified by multiplication by $\pi/4$ for circular arrays and conical scan systems.

If the scanning system is a planar array, this formula can be shown to lead to a scan condition that determines the minimum element (or subarray) size in order to achieve the required economy. Assuming a rectangular array of elements with rectangular cross section $d_1 \times d_2$, with zero wall thickness, and assuming uniform illumination and principal plane beamwidths of approximately λ/d_1 and λ/d_2 then for an array consisting of the minimum number of phase controls as given by Eq. (1), one notes that the following condition must be satisfied in each principal plane:

$$(d/\lambda) \ \sin \theta_{max} = 0.5$$ (2)

Note that the incremental phase shift necessary to scan to this limit is 2π times this number and so the scan condition can never be achieved with an array using symmetrical element patterns because the 180° incremental phase shift would produce two beams of equal size. However, the equivalence of this condition for planar arrays, together with the equation defining the minimum number of elements (which is used for planar arrays or other scan systems), allows a convenient tool for comparison.

For example, an array that is designed to scan to $(d_1/\lambda) \sin \theta'$ and $(d_2/\lambda) \sin \theta^2$ and which requires "Q" phase controls per element for beam steering and pattern control, will have an element use factor of

$$\frac{N}{N_{min}} = \frac{Q(0.5)^2}{\left[(d_1/\lambda) \ \sin \theta^1\right] \left[(d_2/\lambda) \ \sin \theta^2\right]}$$ (3)

7

Equation (3) will be used throughout the report for comparing various approaches.

The advantage of assuming this point of view is that most limited scan antenna types have relatively fixed element use factors, and so one can directly compare very different types of systems using this mechanism. Arrays scanning offset reflectors can have factors between 2 and 3 if properly designed, whereas arrays scanning dual-reflector or lens systems can have factors as low as 1.4 (although requiring the use of relatively large subreflectors). A conventional array with 0.5λ spacing, scanned to 10° in each plane, would have an element use factor of about 33 and thus require that many times the minimum number of phase controls. Its factor is unity if scanned to end-fire. Arrays with fixed spacing (independent of maximum scan angle), do not take advantage of the scan restriction but the technique discussed in this paper is a true limited scan approach because the element size is increased as maximum scan is decreased in order to maintain constant element use factor, and thus to take advantage of the scan reduction by decreasing the number of phase controls.

A previous paper[7] introduced a technique for using large aperture elements in a limited scan array. Grating lobe reduction was achieved by control of the amplitude and phase of a higher order odd mode in order to produce an element pattern null at the nearest grating lobe in the plane of scan. Preliminary data showed that this technique could provide grating lobe suppression of up to

$$d_y/\lambda \sin \theta = 0.6 \tag{4}$$

for E-plane scan using horn aperture elements with two phase controls per horn. Some data were also given for H-plane scan, and it was observed that in this plane one must either tolerate higher grating lobes at broadside, or decreased scan limits. The earlier paper also presented a demonstration that random errors in odd mode power amplitude do not alter the position or depth of the element pattern null.

These early results were obtained using theoretical array data and some experimental element pattern data, and the later survey[3] showed some data for an 8-element array for E-plane scan. These earlier works did not address the important issues of sidelobe suppression, bandwidth, and the realization of circuits for scanning in two planes. This paper presents new results that demonstrate the use of multiple mode control for array grating lobe suppression, that outline the advantages and disadvantages of using this technique for two planes of scan, and that demonstrate control of far grating lobes by the use of dielectric layered filters and by column or row displacement.

8

The present data indicate that the multimode approach, when combined with a new technique for sidelobe control using spatial filtering, can achieve approximately -20 dB sidelobe levels, extremely good aperture efficiency, and requires only 2.5 to 3 times the theoretical minimum number of phase controls for a given gain and scan sector. This required number of phase controls is approximately the same as for most array-reflector limited scan systems[3] which occupy a much larger volume and require perhaps double the final aperture. Limitations of the technique at its present state of development are its bandwidth and the requirement for a spatial filter to obtain the -20 dB sidelobe level.

2. ODD MODE CONTROL FOR SCANNING IN THE E-PLANE

2.1 Element Pattern Scanning

Element pattern data presented in the previous paper showed that substantial grating lobe reduction could be achieved by forming an element pattern null and controlling it as a function of array scan. The element pattern data at a given fixed frequency showed that deep nulls could be maintained for scan angles up to the stated limit $(d_y/\lambda) \sin \theta_{max} = 0.6$ (see Figure 1) and that this could be achieved consistent with gain reduction of about 1 dB at maximum scan angle.

The required odd mode amplitude and phases are obtained from a knowledge of the element patterns for even and odd modes. An array for E-plane scan, as depicted in Figure 1 with $\Delta_n = 0$, has its field pattern given by
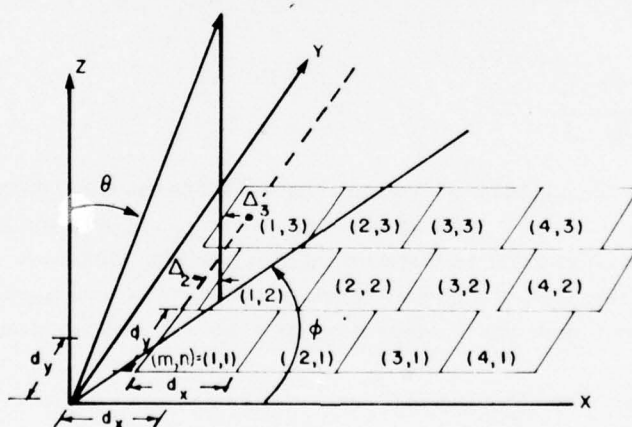

Figure 1. Array Coordinates (Element Center Locations $x = md_x + \Delta_n$, $y = nd_y$)

9

$$E(u, v) = E_x(u) \sum_{n=1}^{N_y} I_n^E \, e_y(v) \, e^{j \frac{2\pi}{\lambda} (v - v_o) n d_y} \; . \tag{5}$$

Here $E_x(u)$ is the array H-plane radiation pattern, I_n^E is the amplitude coefficient at the nth element, and the phase has been chosen to form a beam at $v = v_o$. The direction cosines u and v are given by:

$$v = \sin \theta \sin \phi$$
$$u = \sin \theta \cos \phi \; . \tag{6}$$

The E-plane distribution has grating lobes at

$$v = v_o + q\lambda/d_y.$$

The element pattern $e_y(v)$ is zero at the grating lobe positions $v = \pm q\lambda/d_y$ corresponding to broadside main beam position for a uniformly illuminated element. The growth of the $q = -1$ grating lobe as a function of scan can be nearly eliminated by actively controlling $e_y(v)$ to place a zero at this grating lobe for all scan angles. In a waveguide circuit such control is accomplished by exciting the aperture with two modes (the LSE_{10} and LSE_{11}) instead of just the dominant LSE_{10} mode, so that $e_y(v)$ becomes the sum of two terms, with a zero at the appropriate angle. Defining the ratio of odd mode to even mode as R_{11}, one notes that the combined element pattern

$$e_y(v) = e_{y_o}(v) + R_{11} \, e_{y_1}(v) \; . \tag{7}$$

Upon choosing $e_y(v)$ to be zero at the position of the $q = -1$ grating lobe, one obtains for R_{11}

$$R_{11} = \frac{-e_{y_o}(v_{-1})}{e_{y_1}(v_{-1})} \tag{8}$$

Since the various waveguide modes have constant phase aperture distribution, e_{y_o} is a real function and e_{y_1} is pure imaginary, so the R_{11} is pure imaginary and increases with scan in order to maintain the null position coincident with the center of the $q = -1$ grating lobe. The relative odd mode phase is thus fixed at $\pm 90^o$ with respect to the even mode phase, depending upon the sense of the scan angle.

2.2 Control Circuits

Several types of circuits were described in the previous study for dividing the power between the even and odd mode signals. The basic control circuit (Figure 2a) uses two hybrids and two phase shifters in a conventional power divider to form the
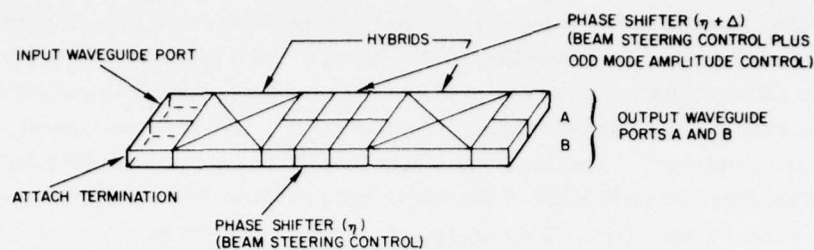
10

Figure 2. Basic Power Divider Circuits

input signals of a monopulse-type network (not shown) that excites the even and odd modes. This circuit has the advantage of exciting the even and odd modes at separate terminals, and allows the use of a short horn structure since the relative odd mode-even mode phase difference of 90° which must be maintained at the aperture can be adjusted using the lengths of lines feeding the separate ports. The extra short horn structure makes bandwidths in excess of 10 percent reasonable.

An alternative circuit (Figure 2b), is simpler because two hybrids are eliminated and the junction into the dual mode waveguide takes the place of one of the hybrids, providing model terminals that correspond to a sum and difference port. Although possessing the advantage of simplicity, this circuit has the disadvantage of requiring an extra length of L dual mode waveguide sufficient to align properly the even and odd modes in the aperture. This dispersive length of line thus introduces the major bandwidth limitation of the array.

2.3 Array with Dielectric Lenses

The experimental and theoretical patterns used in the earlier study filled in to about the -15 dB level, whereas the theoretical patterns had perfect nulls. This null filling was due to the phase distortion in the flared horn aperture and caused

11

grating lobes to exist at the filled level even for broadside radiation. Figure 3 illustrates the use of a lens to collimate the beam of each horn; Figure 4 shows the broadside pattern data for an array of 8 E-plane horns equipped with polystyrene collimating lenses and excited with an illumination to produce approximately -19 dB near sidelobes. The lens, as described,[11] has a flat back face and curved front face protruding out of the horn, and produces less aperture taper than one with a curved back face. This design is therefore preferred since element pattern broadening directly results in increased grating lobes for the broadside main beam. Each lens face was matched at 11.25 GHz using quarter-wave matching ridges. The horn elements were excited by 0.874 in. square waveguides and are 7.5 in. long. The E and H-plane aperture dimensions are 3.11 in. and 1.825 in. The lenses are made of Plexiglas ($\epsilon = 2.6$) and are 0.84 in. thick including the quarter wave ridges. The broadside pattern data of Figure 4 shows a comparison of the radiation patterns of an 8-element array with and without lenses. The figure shows some asymmetry in its pattern distribution, but clearly demonstrates that the grating lobes nearest broadside can be reduced between 4 and 5 dB using the lens design. Figure 5 shows the grating lobes at maximum scan and indicates that levels of about -14 dB are achieved with the lens geometry even in that case.

The key development in the above description is that the lobes nearest broadside can be reduced to the -18 dB level and, with care, to levels below this. This fact is crucial to the design of large elements for limited scan because there are no other techniques available for reducing grating lobes located near to broadside except the use of random element placement. As indicated in Figure 5, other

MATCHED CONVEX
DIELECTRIC LENS FOR
BROADSIDE COLLIMATION

PHASE SHIFT η
(BEAM STEERING CONTROL)

|← L →|

PHASE SHIFT $\eta + \Delta$
(BEAM STEERING CONTROL PLUS
ODD MODE AMPLITUDE CONTROL)
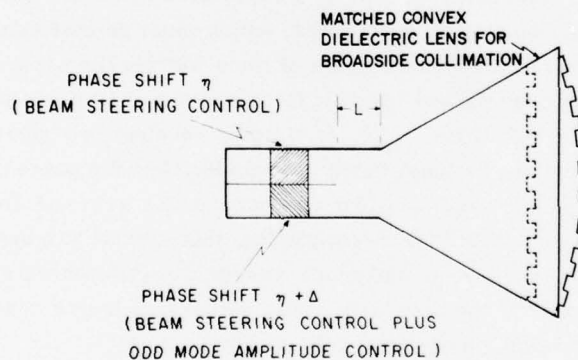
Figure 3. Array Element with Lens

11.   Zahn, L. (1974) Design of a Collimating Lens for a Limited Scan Array, AFCRL-TR-74-0492, Physical Sciences Research Papers, No. 223.

12
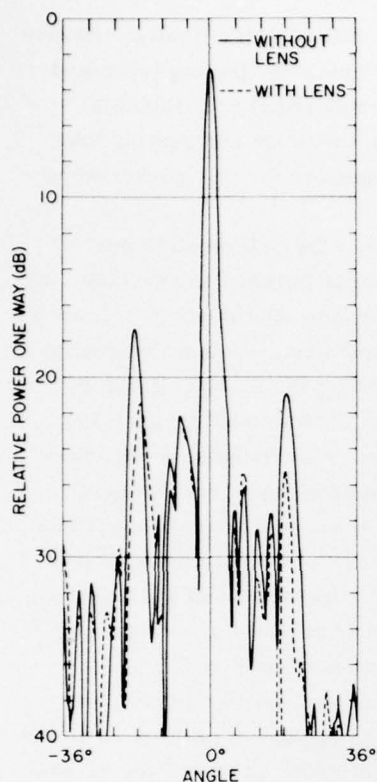
Figure 4.   Broadside Data:
Array with Lenses
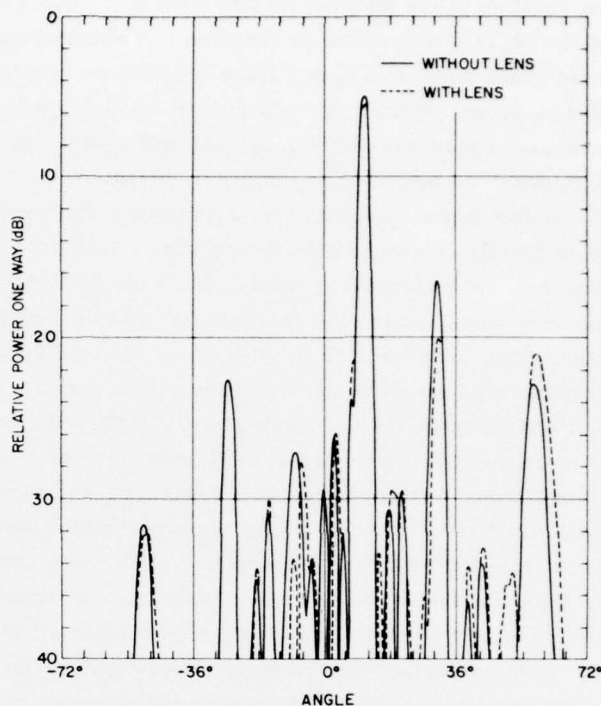
Figure 5.   End-of-Scan Data: Array
with Lenses

grating lobes do increase when the array is canned, but they are never very near
to the broadside direction and so can be suppressed by other means.   These will
be called the "far grating lobes" and techniques for suppressing them are discussed
later.   The collimating lenses perform the one crucial task of assuring that these
near broadside grating lobes are sufficiently suppressed.

The cross polarized radiation of this array was measured at less than -19 dB
relative to the main beam for the maximum scan (worst case) situation, as com-
pared with about -22 dB without the lenses.

The element pattern null formed and controlled as a function of scan suppresses
the largest grating lobe.   The position of this null is determined by the ratio of odd
mode to even mode signal as indicated in Eq. (8), and this ratio is related directly
to the difference in phase provided by the two phase shifters in the odd mode power
divider.   When chosen correctly at the center frequency, this null corresponds to

13

the position of the nearest grating lobe (q = -1). The null remains fixed in position on the $(d_y/\lambda)\sin\theta$ curve as frequency is changed and since the grating lobes and main beam also remain in a fixed position on this normalized curve, the null always occurs at the grating lobe. Thus, even though the beam and grating lobe positions squint with frequency, the null squint compensates for this phenomenon to provide the potential of wideband operation.

Although the null position is frequency independent, the null depth is not. It is primarily determined by the relative phase differences between the even and odd modes in each element aperture, and waveguide dispersion thus imposes a limit on the accuracy to which the required 90° can be maintained over a given frequency band. This bandwidth is much larger for circuits fed by hybrid power dividers (Figure 2a) than those which utilize the waveguide dispersion itself (Figure 2b) to align the even and odd mode phases at the aperture. Figure 6 shows the measured null depth for the array of Figure 7. These elements were not designed to be broadband and are excited by dual mode waveguides whose dispersion accounts for almost all of the null filling observed in this figure. The same horns without the attached waveguides have only slightly more than a degree of phase dispersion between the even and odd mode phases over a 10 percent bandwidth, and so the geometry of Figure 2a can be used if broader bandwidths are desired.

Another factor that influences observed null depth as a function of frequency is the excitation of unwanted higher order modes at the apertures, lenses or in the horn throats. No attempt was made to suppress these modes in any of the several horn types studied during this experimental program and one could observe these contributions filling in the scanned null to levels of nearly -16 dB. This effect can be avoided at any one frequency, but re-enters periodically as frequency is varied. Its reduction below this level depends upon good lens matching and care taken in exciting the desired higher order mode.
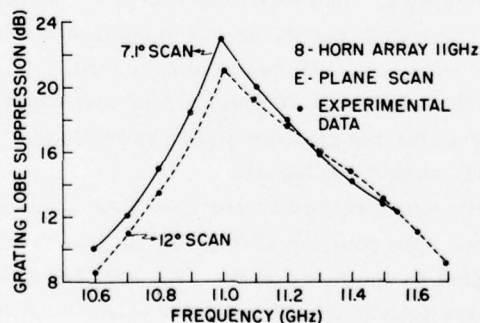
Figure 6. Null Depth Bandwidth

14
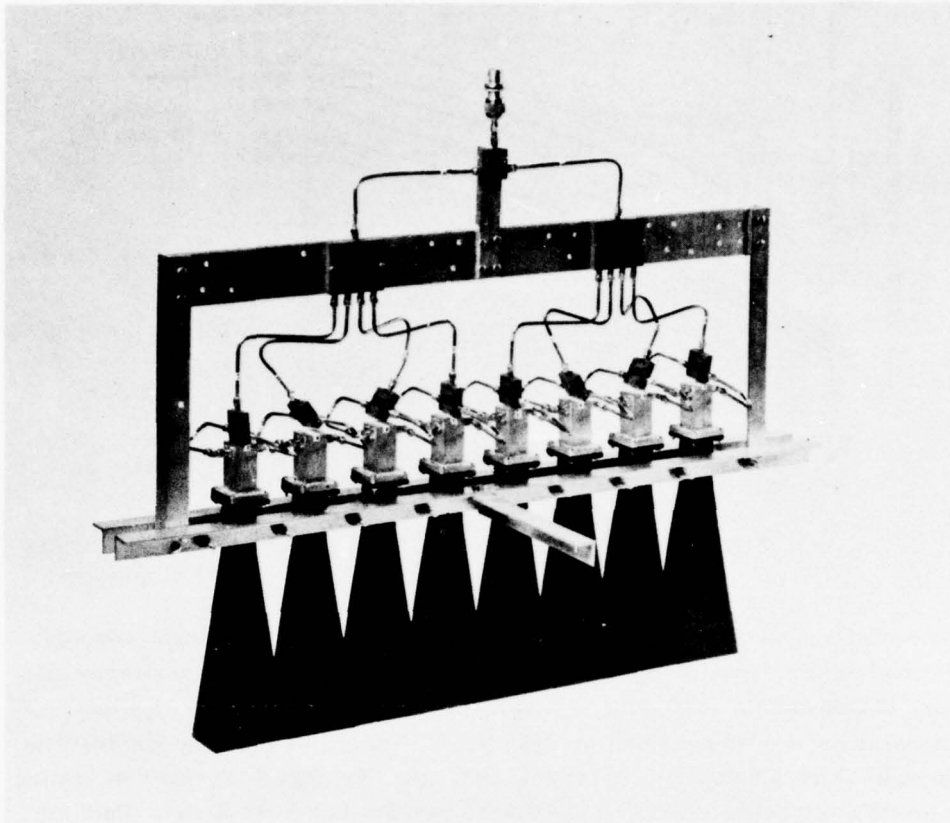
Figure 7. Eight-Horn Prototype Array

2.4 Maximum Achievable Null Depths

Assuming that each of these factors can be controlled, so that the even and odd element patterns combine exactly to form a perfect null at the principal grating lobe, one observes that the suppression provided at this lobe still depends upon the width of the null compared to the array beamwidth. For any given size array, this means that using low sidelobe array distributions has the adverse effect of broadening the beam, and thus decreasing the effectiveness of a given element pattern null in suppressing the principal grating lobes. Figure 8 shows several examples of the maximum suppression achievable for the $q = -1$ grating lobe at broadside and at the end-of-scan assuming Chebyshev array distributions with sidelobe levels of -20, -30, and -40 dB. These data are based upon calculations assuming ideal E-plane element patterns, and show that 20 dB grating lobe

15
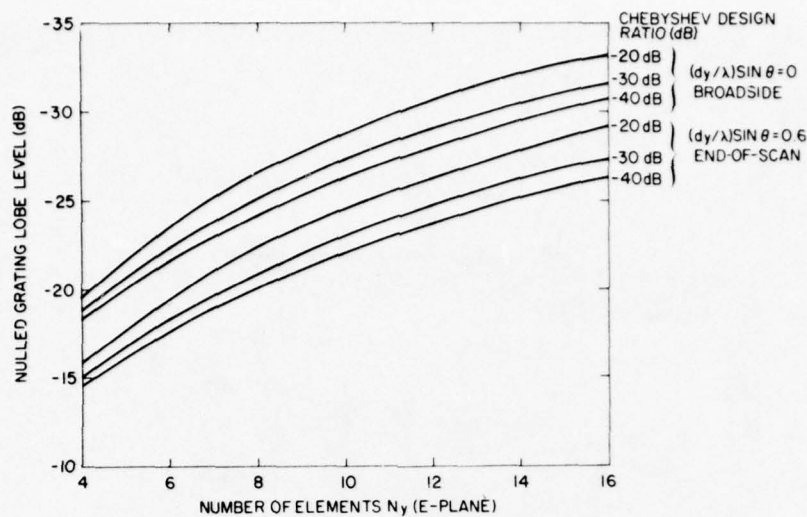
Figure 8. Grating Lobe Level vs Array Size

suppression is achievable, even with -40 dB near sidelobes, for arrays with eight or more elements disposed along the scan plane. The requirement of a minimum number of elements is seen as no limitation for -20 dB sidelobes because the technique is not needed for small arrays, and has its most significant applications to cases in which the number of elements is large. The data do reveal that grating lobe levels much below -25 dB can only be achieved with a large array. Data for uniform amplitude have not been included in the figure because in that case the grating lobe levels are submerged in the sidelobe structure.

3. EXPERIMENTAL RESULTS FOR H-PLANE AND DUAL PLANE SCAN

3.1 H-Plane Scan

As shown in Section 2, the multimode scanning technique is ideally suited to E-plane scan because the array grating lobes lie in the element pattern nulls when the array is at broadside. The H-plane scan offers more difficulties because the widened element pattern has nulls beyond the grating lobe points for the array at broadside, and so energy is lost into these H-plane grating lobes. Figure 9 shows the H-plane experimental element patterns for several scan conditions for a flared horn with and without dielectric loading. These curves have been normalized so that their peaks are at the same level, and this precludes their use for gain comparison. The vertical lines denote the main beam and grating lobe positions

16
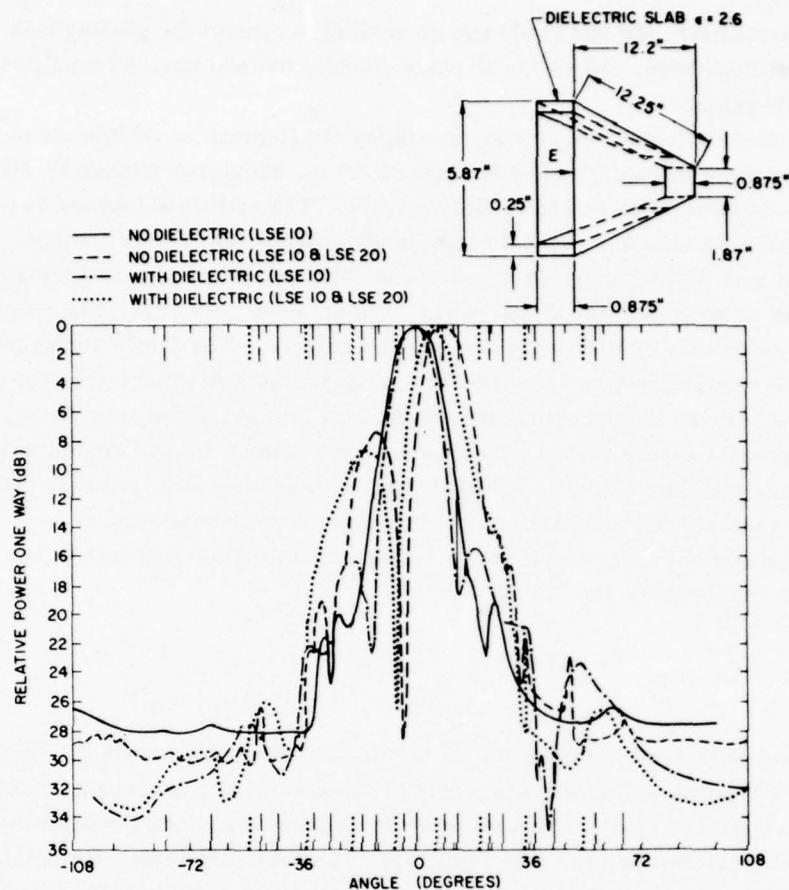
Figure 9. H-Plane Correction Using Dielectric Slabs

corresponding to any given scan angle. Observed grating lobe levels for an
unmodified flared horn are indicated on the solid curve of Figure 9 as approximate-
ly -10 dB with respect to the main beam for 4.38λ horn described by Mailloux and
Forbes.[12] The dashed curve of Figure 9 shows that this pattern null is varied
correctly by introducing the H-plane odd mode (LSE_{20}), with $(P_{odd}/P_{total}) = 0.6$,
and that in fact the null can be controlled well beyond the $(d/\lambda) \sin\theta = 0.6$ point
(to 0.69) at the expense of a -10 dB grating lobe at $\sin\theta = \sin\theta_o - 2\lambda/d_x$ for a
main beam at θ_o.

12. Mailloux, R.G., and Forbes, G.R. (1973) Experimental Studies of a Multiple
    Mode Array Technique for Limited Scan Application, AFCRL-TR-73-0685,
    Physical Sciences Research Papers, No. 575.

17

Unfortunately, the odd mode can do nothing to control the grating lobe level present at broadside, and so the H-plane element pattern must be modified for proper operation.

The dash-dotted curve of Figure 9 shows the H-plane broadside element pattern of the 4.38λ (5.87 in.) horn using 0.25 in. Plexiglas dielectric slabs at the H-plane horn walls as shown on the figure. The slabs are tapered to nearly a point to affect a smooth transition into the dielectric loaded horn section. This geometry was developed by Tsandoulas and Fitzgerald[13] to improve the aperture efficiency of large H-plane flared horns, and achieves this efficiency by making the field wave more uniform throughout the aperture. The figure shows that the broadside element pattern is indeed improved by this design, for the near grating lobes are reduced to approximately -18 dB with respect to the main beam. The dotted curve of Figure 9 shows the geometry provides a controlled null suitable for scanning to $(dx/\lambda)\sin\theta = 0.49$, but that the p = -2 grating lobe is larger than the E-plane case and its suppression remains a problem to be solved.

The H-plane odd mode excitation for the circuit using dielectric slabs is given by direct analogy with Eq. (8) as:

$$R_{20} = -e_{x_1}(u_{-1}) / e_{x_2}(u_{-1}) \ . \tag{9}$$

Cross-polarized radiation for E- and H-planes was below -24 dB for the even mode in either case; the odd modes had cross-polarized components of -24 and -20 dB for the two cases. These low cross-polarized radiation components offer good assurance that the linearly polarized LSE modes are indeed the dominant higher order modes excited, and that cross-polarized radiation effects can be neglected for all but extremely low sidelobe requirements.

3.2 Scanning in Two Planes

Having thus achieved scanning in both principal planes, one observes that it is not difficult to anticipate the characteristics necessary for scanning in two dimensions. The array of Figure 1 has the field pattern given below; the basic phase controls are chosen to form a beam at (u_o, v_o) in direction cosine space:

13. Tsandoulas, G.N., and Fitzgerald, W.D. (1972) Aperture efficiency enhancement in dielectrically loaded horns, IEEE Trans. AP AP-20 (No. 1): 69-74.

18

$$E(u, v) = \frac{1}{N} \sum_{m=1}^{N_x} \sum_{n=1}^{N_y} I_{mn} \, e(u, v)$$

$$\times e^{j\frac{2\pi}{\lambda}\left[(v-v_o)nd_y + (u-u_o)(md_x + \Delta_n)\right]} \tag{10}$$

where $u = \sin\theta\cos\phi$ and $v = \sin\theta\sin\phi$ and where I_{mn} is the amplitude of excitation at element (m, n). Assuming that the array is excited by a separable distribution so that $I_{mn} = I_m^H I_n^E$, and assuming that the element pattern is also separable, then $e(u, v) = e_x(u) e_y(v)$, one can write this field distribution in the following form:

$$E(u, v) = \frac{1}{N_x} \left\{ \sum_{m=1}^{N_x} I_m^H \, e_x(u) \, e^{j\frac{2\pi}{\lambda}(u - u_o)md_x} \right\}$$

$$\times \frac{1}{N_y} \left\{ \sum_{n=1}^{N_y} I_n^E \, e_y(v) \, e^{j\frac{2\pi}{\lambda}\left[(v-v_o)nd_y + \Delta_n(u - u_o)\right]} \right\}$$

$$= E_x(u) \, E_y(u, v) \quad . \tag{11}$$

This pattern is not separable in general, but may be so for certain choices of $[\Delta_n]$. The choice of optimum $[\Delta_n]$ for grating lobe reduction will be considered later. If $[\Delta_n] = 0$, the field pattern is separable and is written:

$$E(u, v) = \frac{e_x(u)}{N_x} \sum_{m=1}^{N_x} I_m^H \, e^{j\frac{2\pi}{\lambda}(u - u_o)md_x}$$

$$\times \frac{e_y(v)}{N_y} \sum_{n=1}^{N_y} I_n^e \, e^{j\frac{2\pi}{\lambda}(v - v_o)nd_y}$$

$$= E_x(u) \, E_y(v) \quad . \tag{12}$$

Maintaining a separable element pattern as required for the control of grating lobes for general scan angles requires the control of an additional waveguide mode, the LSE_{21}. Relative odd mode amplitudes as given by Eqs. (8) and (9) provide

19

control for principal plane scanning, and by exciting the LSE_{21} mode with relative amplitude

$$R_{21} = R_{20} R_{11} , \tag{13}$$

one obtains the following element pattern (using separable horn element patterns)

$$e(u, v) = \left[e_{y_o}(v) + R_{11} e_{y_1}(v) \right] \left[e_{x_1}(u) + R_{20} e_{x_2}(u) \right] = e_y(v) e_x(u) . \tag{14}$$

This separable element pattern, which can be obtained using the circuit of Figure 10, provides excellent grating lobe control for general scan planes. Here each horn is excited by a large waveguide bifurcated in the H-plane to form two waveguides, each capable of supporting the LSE_{10} and LSE_{20} modes. This bifurcated guide is then excited by four waveguides through a power divider network (using 180° hybrids) that forms all symmetry combinations. This circuit excites the basic horn with the four fundamental symmetries as appropriate for proper modal selection. Terminal 1 excites the aperture with an inphase distribution corresponding to the LSE_{10} mode, terminal 2 excites the LSE_{20} mode, terminal 3 the LSE_{11}, and terminal 4 the LSE_{21} mode. Extra line lengths may be added
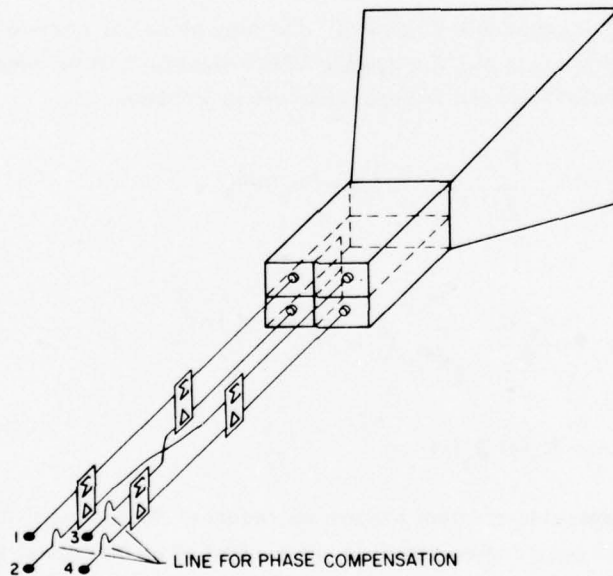

Figure 10. Two Dimensional Horn Excitation

20

to any three terminals to compensate for the phase velocity differences in the horn and produce deep element pattern nulls for any generalized scan angle as well as the principal planes. This circuit can then be excited using another network of four power dividers in an orientation reversed from the ones shown. This network serves as a variable power divider so that if excited by four inphase signals it forms an output at terminal one only, and if excited by four equal amplitude phased signals, it resolves the combined signal down to its four symmetrical components, and excites terminals one through four with the proper amplitude. These circuits are directly analogous with those for one plane of scan and so will not be described further.

In general, the circuit of Figure 10 is preferable to one that would be the two-dimensional equivalent of Figure 2b because of the bandwidth limitations imposed by using the difference in waveguide propagation constants to correct the relative phases of the four modes. The modal parts of Figure 10 are separate and one can make length corrections external to the multimode waveguide structure.

The results obtained in an experiment using this circuit are shown in Figures 11 and 12 for a single horn element with dimensions given below. The horn is loaded with dielectric slabs to narrow the H-plane beamwidth.

$$\frac{d_y}{\lambda} = 4.58$$

$$\frac{d_x}{\lambda} = 3.44 \quad .$$

The circuit of Figure 10 was configured using strip-line power dividers and interconnecting coaxial lines, but the power division network for forming the input signals to ports 1 through 4 was configured externally using phase shifters and attenuators. Duplication of these experiments using a variable power divider controlled by phase shifters is seen as providing no additional difficulty.

The use of an H-plane bifurcated guide as indicated in Figure 10 instead of a large multimode waveguide at the horn throat is warranted because when the four waveguides are used directly at the throat, the excitation of the LSE_{21} mode produces a cross-polarized component that is even in azimuth and elevation. This contribution was measured at approximately -18 dB relative to the peak of the beam, but it is suppressed to about -23 dB using the H-plane bifurcation.

A second factor which influenced the way the experiment was conducted is that the coordinates of the array grating lobe positions coincide with the pattern cuts that are taken with an elevation-azimuth antenna mount only when the lobe positions coincide with one of the principal planes, and since that condition was

21
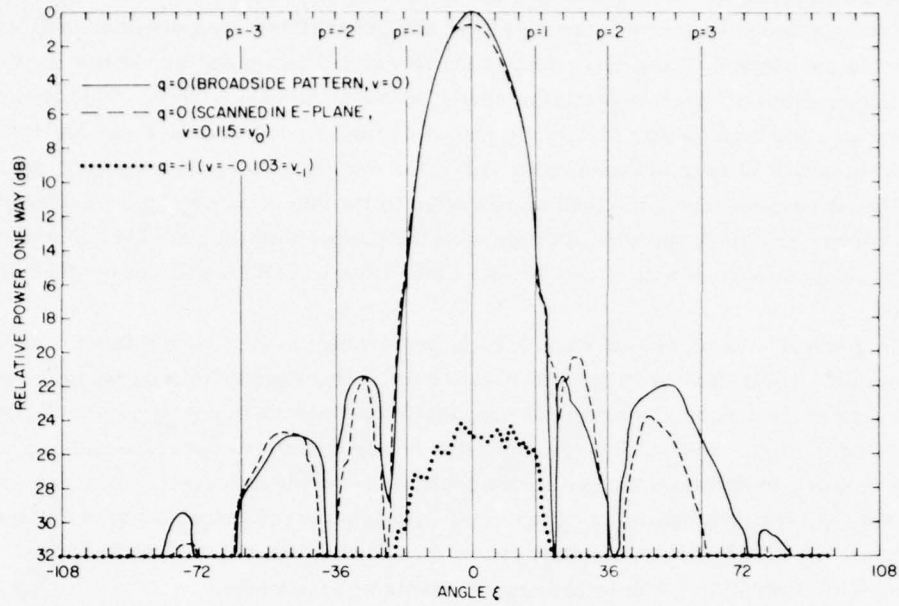
Figure 11. Experimental Results: Two Dimensional Horn
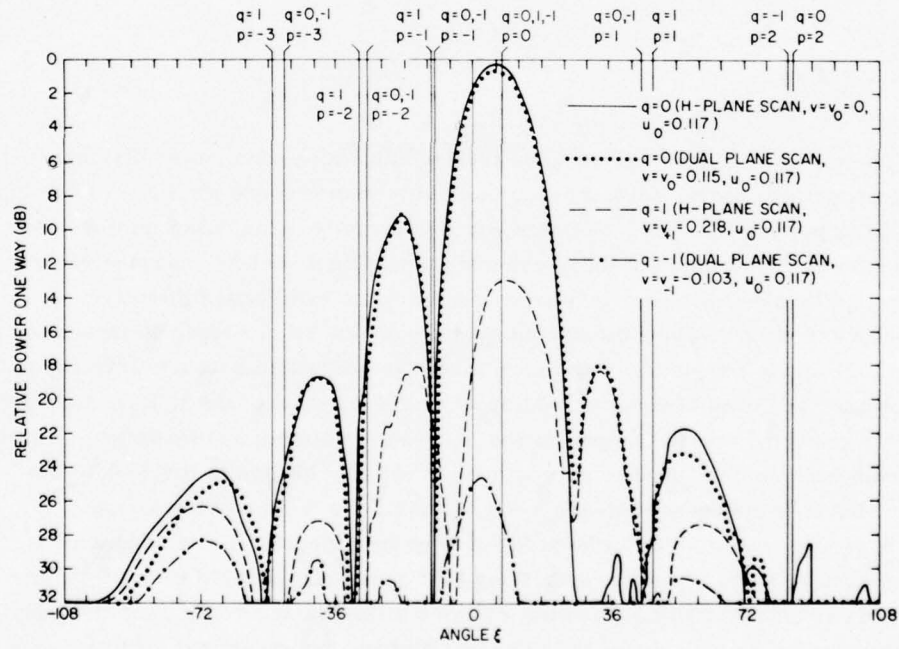
Figure 12. Experimental Results

22

seldom fulfilled in this experiment, the lobe positions are displaced from the azimuth positions. Figure 13 shows the relationship between the array coordinates and the pattern mount coordinates. The direction cosines u and v are related to the mount coordinates by the relations

$$u = \cos \eta \sin \xi$$
$$v = + \sin \eta \quad . \tag{15}$$

These equations show that in the principal planes, when $\eta = 0$ or when $\xi = 0$, these ξ or η components assume the function of the original ϕ and θ array coordinates; and thus grating lobes in the planes $\phi = 0$ and $\phi = \pi/2$ lie along the principal planes of the antenna mount. Fortunately, the elevation angle η depends only upon the direction cosine v, so it is convenient to take azimuth cuts (ξ) through the specific elevation planes (η) which correspond to the v_q grating lobe positions. The u_p grating lobes are thus located in that elevation plane at angles ξ_{pq} according to the relationship:

$$\xi_{pq} = \sin^{-1} \left[\frac{u_p}{\sqrt{1 - v_q^2}} \right]. \tag{16}$$
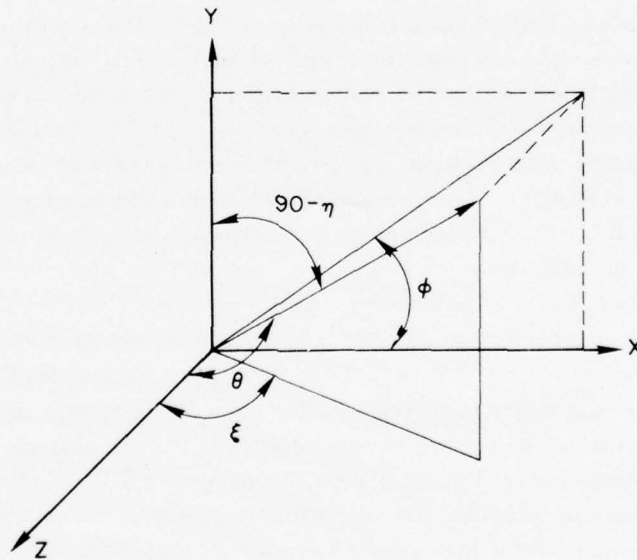
Figure 13. Antenna Pattern Mound Coordinates

23

This azimuthal displacement correction has been applied to all of the recorded grating lobe positions. Figure 11 shows the H-plane pattern of a single horn with only the LSE_{10} mode excited. The grating lobe positions are marked by vertical lines. Those indicated at ±1 grating lobes are evidently suppressed about 15 dB relative to the main beam. Obviously these lobes could have been further suppressed by narrowing the element pattern using thicker dielectric loading or a higher dielectric constant, but the chosen configuration was selected because it has better scanning characteristics than a heavily loaded horn. The cross polarized component of this radiated mode is below -34 dB everywhere in space. Figure 11 also shows two H-plane patterns of the basic horn element scanned in the E-plane by the addition of the LSE_{11} mode. The dashed pattern is taken through a cut denoting the main beam location at 6.6° ($v = 0.115$) away from broadside in the E-plane, and the dotted pattern is an H-plane cut taken through the E-plane grating lobe locations. The dashed figure shows a power loss of about 0.7 dB in scanning the element to this elevation point $(D/\lambda) \sin \theta = 0.53$ which is slightly less than maximum scan. This loss is measured through the power dividing network and should not be interpreted as an absolute gain number. The shape of the pattern is nearly identical to the broadside pattern, indicating that the u_p lobe suppression is not deteriorated by scanning in elevation. The dotted pattern is an H-plane cut through the null formed in the elevation plane ($v_{-1} = 0.103$) and occurs at -5.9°. The largest grating lobe indicated in this pattern cut is at -24 dB relative to the main beam. Cross polarized radiation for this case was measured at -29 dB.

Figure 12 shows four H-plane cuts representing various conditions that include H-plane scan and scan to an intercardinal plane. The vertical lines mark azimuthal grating lobe locations for each elevation. The solid and dashed curves are taken at different elevations for the element excited with the LSE_{10} and 20 modes to achieve for H-plane scan. The solid curve is taken at zero elevation and has its null at -10° (u_{-1}) corresponding to a main beam angle of 6.7° ($dx/\lambda \sin \theta = 0.40$). The null formed by this pattern is at approximately -21 dB with respect to the main beam, and the gain measured through the dividing network is approximately 0.4 dB below the main beam level for broadside radiation (Figure 11). Other grating lobes in this principal plane are at levels below -16 dB. The dashed curve of Figure 12 is an azimuthal cut through the plane with elevation angle 12.6°, corresponding to the v_1, grating lobe. This pattern has a peak about -12.5 dB below that of the pattern at zero elevation; it is an example of the same E-plane null filling observed in the previous experiments with E-plane scan. As before, this level can be reduced using collimating lenses, but no attempts have been made to design such a device for a horn loaded with dielectric slabs as required for H-plane scan control. The appearance of the pattern at this elevation is similar to that at zero elevation, but the null is displaced so that it no longer

24

corresponds to the p = -1 grating lobe. This is due to the presence of higher order modes resulting in imperfect separability of the 10 and 20 patterns in the region of their elevation nulls, and consequently in a grating lobe (p, q = -1, 1) about -21 dB relative to the main beam. The cross polarized component was measured at -29 dB relative to the main beam.

The dotted curve of Figure 12 is the azimuth pattern at the elevation angle 6.6° for the horn with modes 10, 20, 11 and 21 chosen to form a beam at 6.6° elevation and 6.7° azimuth. The main beam gain is approximately 0.9 dB below the level of the broadside pattern but otherwise the pattern is nearly identical to the case for pure H-plane scan (solid curve) at zero elevation angle. Figure 12 illustrates the good quality of grating lobe suppression achievable in two dimensions, because comparison with the dash-dotted curve taken at the E-plane null (-5.9°) demonstrates that about -30 dB suppression is achieved for the nearest E-plane grating lobe, and the primary H-plane lobes are suppressed below that level. The E-plane cut through v_{-2} is not recorded here, but is consistent with the -12 to -13 dB levels observed for all other E-plane scan conditions. The cross-polarized radiation is at approximately -23 dB relative to the main beam.

The main point illustrated by this experimental study is that the patterns formed by the four-mode horn are indeed separable (except near the pattern zeros of each isolated mode), and so one can combine modes using the power ratios that are appropriate for the principal planes of scan, and achieve good grating lobe control in two planes. This separability is evidenced in both figures by the nearly identical azimuth cuts through different elevation angles, and by the fact that the null locations remain stable as *required for good grating lobe suppression.*

4. REDUCTION OF FAR GRATING LOBES

The multimode approach described in earlier sections provides substantial suppression of the large grating lobes nearest broadside, allowing scan to reasonable angles without excessive power loss. As indicated earlier, the scan limit is defined principally by the existence of relatively large grating lobes at (p or q) equal to -2 for a beam scanned in the positive direction in u or v space. These lobes reach -12 to -14 dB in the E-plane and larger in the H-plane, depending upon where the scan limit is defined.

Although these sidelobe levels are acceptable for certain applications, there are many more which require sidelobes at about the -20 dB level. If circumstances permit, this increased suppression of far grating lobes can be achieved by several means, and the task of evaluating the practicality of multimode techniques for any given limited scan system becomes one of determining which, if any, sidelobe suppression scheme applies.

25

Two techniques for far grating lobe suppression have been investigated in this laboratory: (1) the synthesis of dielectric layer spatial filters for grating lobe rejection; and (2) the judicious selection of array lattices for grating lobe suppression in one plane.

4.1 Synthesis of Spatial Filters Using Dielectric Layers

Synthesis procedures have been devised that produce layered dielectric filters with good transmission throughout a specified spatial passband and substantial rejection throughout a stopband region that is made to coincide roughly with the grating lobe locus. The procedure that has been developed[14] synthesizes these filters in terms of Chebyshev polynomials; it has been successful in grating lobe suppression even in the presence of mutual coupling effects at the array face.

Figure 14 shows the radiation pattern of the 8-element array described earlier but using uniform illumination and without lenses. At the end of scan (12°) the array has major grating lobes at about -26°, -51°, $+33^O$ and $+62^O$. The filter that was designed for grating lobe suppression in this case was a four layer
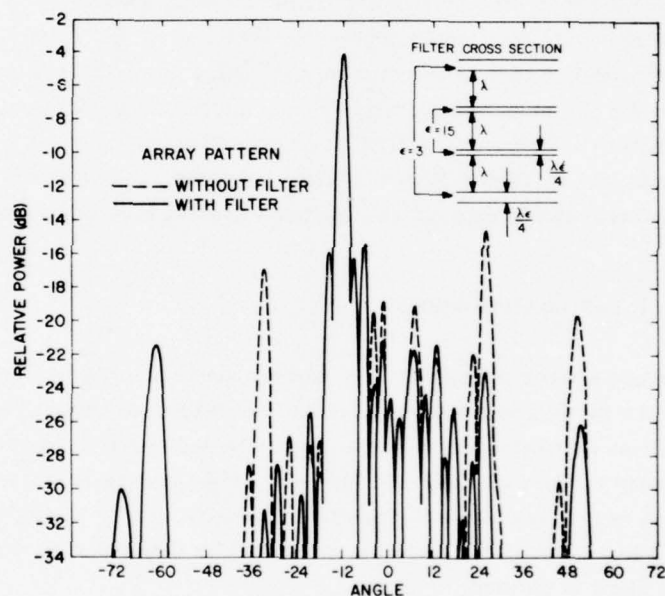

Figure 14. Grating Lobe Suppression by a Spatial Filter

14. Mailloux, R.J. (1976) Synthesis of spatial filters with Chebyshev Characteristics, IEEE Trans. AP AP-24(No. 2):174-181.

26

Chebyshev geometry with quarter wave dielectric layers having dielectric constants 3, 15, 15, and 3 arranged in that order and each separated by one wavelength of a very low dielectric spacer material. The filter dimensions are 3 feet by 1 foot by about 3.7 inches. Center frequency for this design is 11 GHz.

The use of one wavelength spacing between filter elements produces a second passband at 60°, and the brewster angles for dielectrics with constants 3 and 15 are at 60° and 75°, so the filter was clearly not designed to suppress the grating lobe near 60°. The major design goal was to produce sufficient rejection at the dominant grating lobes at -26° and 33°, and the choice of λ separation gave a very steep cutoff between 12° and 26° so that this large lobe could be suppressed sufficiently. Figure 14 shows the array data with filter (dotted) and without it (solid), indicating that there is little or no measured insertion loss for the main beam at 12°, and that the near sidelobes are essentially unaltered by the filter. The grating lobes at -26 and -51° are suppressed approximately 7.5 dB and 6.5 dB, respectively, and the lobe at 33° is suppressed more than 10 dB. The lobe at 62° is essentially left unchanged. These suppression values follow the predicted values very closely, giving assurance that such filters can be designed to specifications that will suit many limited scan applications.

The Chebyshev filter designed for this experiment has the advantageous property of providing graceful degradation of the filter characteristics as a function of frequency. Since the interlayer electrical length is

$$\xi = 2\pi \frac{\delta}{\lambda} \cos \theta \tag{17}$$

the filter has Chebyshev behavior in frequency as well as in $\cos \theta$, with the net effect that the spatial passband becomes narrowest at the lowest frequency. The design procedure is thus reduced to ascertaining that the sector is wide enough to allow good transmission within the arrays scan sector at the low frequency, and narrow enough at the high frequency so that the nearest grating lobe is strongly rejected. The operating bandwidth is smaller for filters whose maximum spatial passband angle is close to the angle of the nearest grating lobe. The bandwidth approaches zero in the limit when these two are coincident; it is a maximum when these two angles are widely separated.

The Appendix gives several expressions for filter bandwidth in terms of the desired rejection at the grating lobe and tolerable rejection (if any) at the low frequency maximum scan angle. The maximum achievable bandwidth occurs for infinitely steep filter rejection skirts. It is given by

$$\frac{\delta}{f_{-1}} = \left[\frac{\cos \theta_m}{\cos \theta_{g1}} - 1 \right] \tag{18}$$

27

where θ_m is the maximum scan angle for the array and θ_{g1} is the angle of the nearest unwanted lobe. The example given in the Appendix predicts about 5 percent bandwidth for the filter described in this report for the limiting case of 6.5 dB rejection and 0.6 dB insertion loss. Improved characteristics are obtained if the filter is operated over narrower frequency limits.

4.2 Selecting Element Lattices for Optimum Scanning

There have been a number of studies showing the reduction of grating lobes using arrays that are aperiodic in one or two planes. In general, these require complex power dividing and phasing systems, but one can achieve a certain reduction of the grating lobes in one plane by merely displacing the rows of an array that scans in two dimensions. Such displacement as indicated in Figure 1 is consistent with excitation by a conventional power divider and with phase controls that are progressive within each row and, except for a displacement term, are also progressive between columns.

Equation (11) shows that by choosing to displace each row of elements by an amount Δ_n with respect to the first row, one obtains an array radiation pattern that is given by the product of the unaltered H-plane pattern $E_x(u)$ and a non-separable E-H plane distribution $E_y(u, v)$, where:

$$E_y(u, v) = \frac{1}{N_y} e_y(v) \sum_{n=1}^{N_y} I_n^E e^{j \frac{2\pi}{\lambda} \left[(v-v_o)n d_y + \Delta_n (u-u_o) \right]} . \tag{19}$$

The maximum value of this pattern is unity and that value is attained at the main beam location $(u, v) = (u_o, v_o)$ for any values $[\Delta_n]$. This pattern also has the same maximum value if $[\Delta_n] = 0$ at the position $v = v_o$ (for all u). Since the total pattern is the product of this distribution and the $E_x(u)$ function, the only major peaks in the combined pattern occur at the grating lobe positions. The v-plane pattern of a uniformly illuminated array ($I_n^E = 1$) with rectangular lattice ($\Delta_n = 0$) has the expected -13 dB sidelobe pattern characteristic of the uniform array. The form of the sum in Eq. (19) allows one to experiment with the choice of the set $[\Delta_n]$ in order to suppress the peak value of $E_y(u, v)$ as a function of v at the various grating lobe positions $u = u_p$. For example, consider an even number of elements in the E-plane (N_y even). A reasonable choice of lattice is the conventional triangular grid function. Choosing

$$[\Delta_n] = (o, d_x/2, o, d_x/2, o, d_x/2, \ldots) ,$$

28

one obtains at the grating lobe positions $p = \pm 1, \pm 3, \pm 5,$ and so on; the results: (apart from a complex constant of amplitude unity, and after explicitly removing the element pattern $e_y(v)$)

$$\frac{E_y(u_p, v)}{e_y(v)} = \frac{1}{N_y} - \frac{\sin\left[N_y \pi (v-v_o) d_y/\lambda\right]}{\cos\left[\pi (v-v_o) d_y/\lambda\right]} . \tag{20}$$

This pattern has a zero at $v = v_o$, and an asymmetrical distribution in $(v = v_o)$ with principal maxima of unity at $(v - v_o) d_y/\lambda = 0.5$.

At the grating lobes $p = \pm 2, \pm 4, \ldots,$ the summation becomes

$$\frac{E_y(u_p, v)}{e_y(v)} = \frac{1}{N_y} \frac{\sin\left[N_y \pi (v-v_o) d_y/\lambda\right]}{\sin\left[\pi (v-v_o) d_y/\lambda\right]} \tag{21}$$

which again is the same distribution as for uniform illumination and $\Delta_n = 0$, and offers no grating lobe suppression.

The distribution chosen in the foregoing thus suppresses the odd grating lobes in *one sector of space* by splitting them each into two lobes and moving each out to a relatively wide angle, where they are reduced by the element pattern $e_y(v)$; the distribution does not alter the even grating lobes at all. This capability of selectively modifying a chosen grating lobe represents an additional degree of freedom that is useful in designing array techniques for limited scan systems.

In order to investigate the potential for grating lobe reduction using this technique, it is convenient to again explicitly remove the element pattern $e_y(v)$ from Eq. (19) and evaluate the integral of the power within the region $-0.5 \le (v - v_o) d_y/\lambda \le 0.5$. After normalizing this total power to the power at the peak of the beam, one obtains for the normalized power per unit length in $(d_y/\lambda)(v - v_o)$ space

$$P_{ave} = \frac{\sum\limits_{n=1}^{N_y} |I_n|^2}{\left(\sum\limits_{n=1}^{N_y} I_n\right)\left(\sum\limits_{n=1}^{N_y} I_n^*\right)} \tag{22}$$

independent of the Δ_n. For uniform illumination this level is $1/N_y$ and so although it may be possible to choose the Δ_n's so as to reduce the peak value of the grating

29

lobe throughout the region specified, the average value will remain constant at the level $1/N_y$ for an array with N_y rows. The maximum available grating lobe suppression using this technique is thus about 9 dB for an 8-row array and 12 dB for a 16-row array, and so on.

Figure 15 shows five curves of $E_y(u_p, v)/e_y(v)$ with various Δ_n and p combinations for an 8-element array. The Δ_n combinations are chosen in a symmetrical manner across the array in order that the final structure have a perfect monopulse null in the ideal situation. As a result of this symmetry, all patterns have a null at $(v-v_o)d_y/\lambda = 0.5$. In addition, all patterns are symmetric about the points $\pm n$ and $\pm (n+0.5)$ for all integer n including n = 0, and so only a restricted sector of the patterns are indicated.

The solid curve of Figure 15 is the result, as mentioned earlier, for $[\Delta_n] = 0$; it exhibits no grating lobe suppression. The displacement

$$\left[\Delta_n\right] = \left[o, \ d_x/2, \ o, \ d_x/2, \ d_x/2, \ o, \ d_x/2, \ o\right] \tag{23}$$
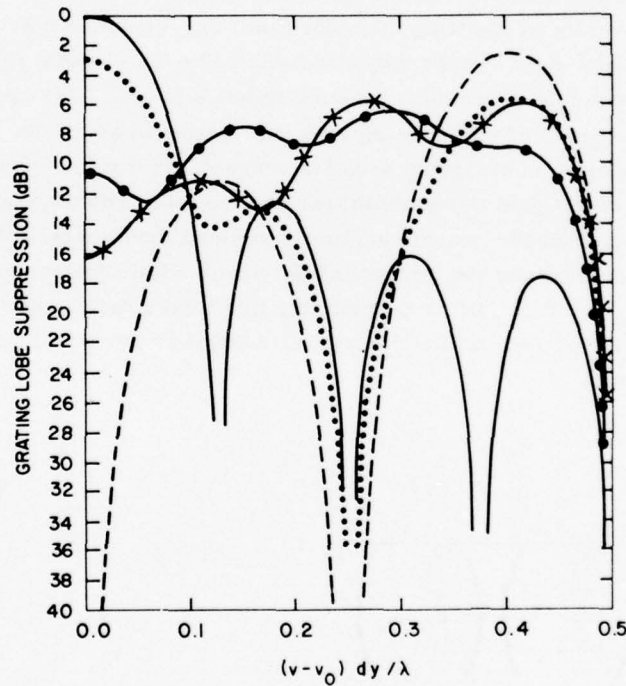

Figure 15. Grating Lobe Suppression by Row Displacement

30

yields the dashed pattern for the grating lobes with $p = \pm 1$ and so has good suppression except near $(v-v_o d_y/\lambda = 0.4$, but the grating lobes for which $p = \pm 2$ again assume the distribution as shown by the solid curve with no suppression.

The displacement

$$\left[\Delta_n\right] = \left[o,\ d_x/4,\ o,\ d_x/4,\ d_x/4,\ o,\ d_x/4,\ o\right] \tag{24}$$

yields the dotted curve shown in Figure 15, and evidently provides only about 3 dB suppression for the lobes with $p = \pm 1$. The grating lobes with $p = \pm 2$ are again given by the dashed curve and so are somewhat suppressed for small $(v-v_o)d_y/\lambda$ values, but have a peak value of -3 dB.

The displacement

$$\left[\Delta_n\right] = \left[o,\ 0.25d_x,\ 0.65d_x,\ 0.85d_x,\ 0.85d_x,\ 0.65d_x,\ 0.25d_x,\ o\right] \tag{25}$$

yields the two solid curves connecting circles $(p = \pm 1)$ and X's $(p = \pm 2)$ shown in Figure 5. This configuration was obtained empirically and provides at least six dB grating lobe suppression throughout space. Although each of these displacement combinations produce the same average (-9 dB) level over the region $-0.5 \leq (v-v_o)d_y/\lambda \leq 0.5$, the last displacement produces the lowest peak grating lobe level and is thus preferred for grating lobe reduction. The second desirable feature about the pattern produced by the above displacement is that it has much more suppression near $(v-v_o)d_y/\lambda = 0$, where the natural element pattern suppression is minimal, and so in some cases one can obtain somewhat more than the 6 dB suppression.

Row displacement can thus provide substantial suppression for most of the grating lobes, but it does not alter those lobes associated with the (u_o, v_n) positions. These beams have the same u - coordinate as the desired main beam, but are displaced in the E-plane. They must be suppressed using dielectric filter techniques or minimized in the design of the basic scanning element. Examples that illustrate the effectiveness of this technique will be given later.

5. CHARACTERISTICS OF DUAL PLANE LIMITED SCAN SYSTEMS

The preceding sections of this report have demonstrated the feasibility of scanning in two planes with the multimode technique. This section is devoted to presenting data that will aid in designing array systems and in evaluating their performance. The tools for this analysis and comparison are the power transmission factors of each element; knowing these, one can add the sidelobe

31

suppression corrections for a spatial filter and row or column displacement, including the array projection factor ($\cos \theta$) to give directivity for a large two-dimensional array and thus compute required performance. The term power transmission factor, as used here, is the ratio of power transmitted in a given direction per unit cell of an infinite phased array to the cell input power. This ratio does not include the beam broadening factor (array projection factor) $\cos \theta$, and for that reason the power transmission factor curves can be used for any size apertures or for column arrays and can provide much more useful information than if this factor were included. Figures 16 and 17 show the power transmission patterns that apply to E- and H-plane scan situations with and without higher order model control. Grating lobe levels for the two-dimensional array are determined by evaluating the levels in these principal planes and forming the product. The curves are plotted in $(d/\lambda) \sin \theta$ space, and so adjacent grating lobes are spaced one unit distance apart in either plane. Thus it is convenient to use these curves for determining the grating lobe levels corresponding to any chosen main beam angle.

These computed element patterns do not include mutual coupling. They were obtained using Eq. (14), and normalizing the levels of these patterns at each scan angle so that the total power was unity. Thus the relative levels at each grating lobe were given by the $e_y(v)$ or $e_x(u)$ functions, but the absolute level was obtained by normalizing the e_x and e_y such that:
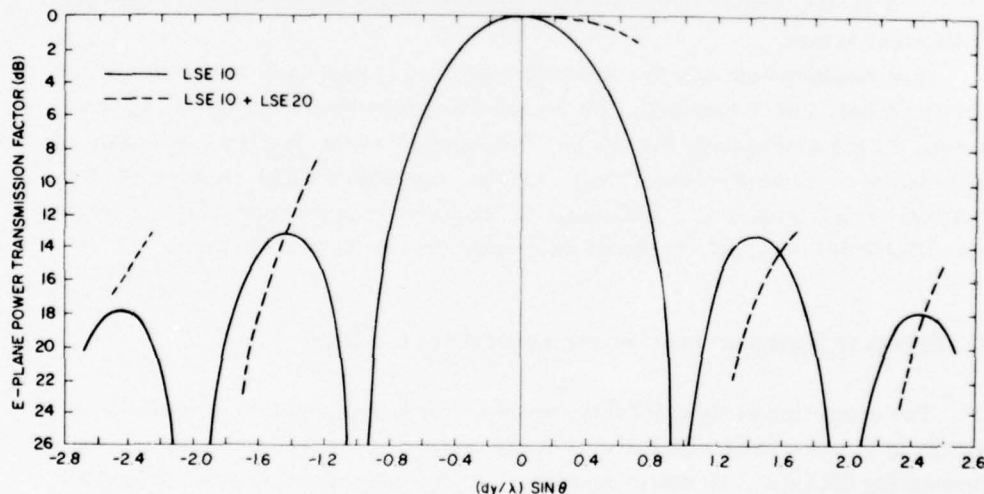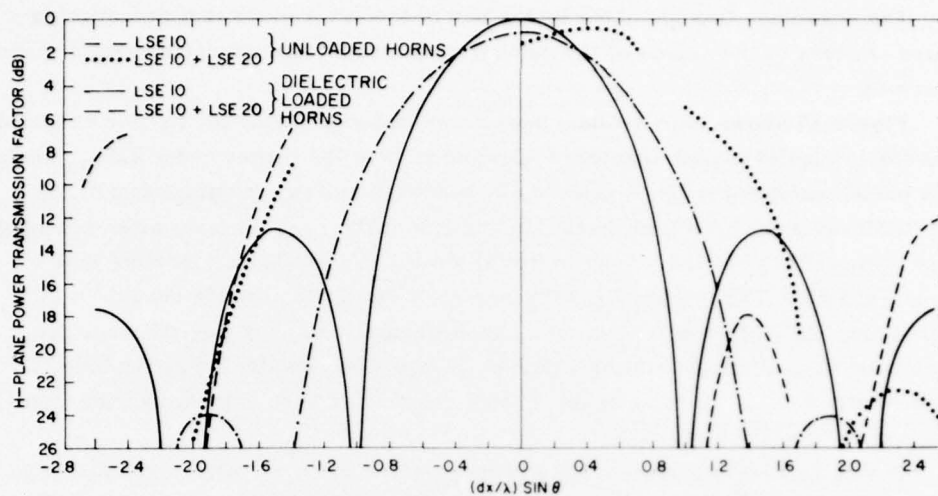

Figure 16. Generalized E-Phase Power Transmission Factors

32

Figure 17. Generalized H-Plane Power Transmission Factors

$$\sum_p \left| e_x^2 (u_p) \right| = 1$$

and

$$\sum_q \left| e_y^2 (v_q) \right| = 1$$

in the principal planes.

For the special case that includes a dielectric loaded waveguide, the $e_x(u)$ was evaluated by solving the required transcendental equation to obtain the wave guide eigenvalue mode numbers, and integrating over the waveguide even and odd mode eigenvalue functions to obtain the radiation field.

Whenever odd modes are used in the control circuit, the element pattern has several discontinuities. These result from the nonsymmetric nature of the actively controlled element pattern, and the point of discontinuity represents the end of scan.

The E-plane data of Figure 16 show the advantage of controlling the higher order mode in this plane. With use of the single mode pattern alone, a beam scanned to $(dy/\lambda) \sin \theta = 0.2$ would have an associated grating lobe level of -13 dB at $(dy/\lambda) \sin \theta = -0.8$. Although at a dangerously steep part of the curve, this would be satisfactory for a large array if some external means of grating lobe suppression were applied. Alternatively, the transmission factor curve using the LSE^{10} and 11 modes (dashed) shows that scan to $(dy/\lambda) \sin \theta = 0.6$ is possible with a resulting grating lobe at about -12 dB.

33

The advantage brought about by the use of the extra mode is a reduction in phase shifters to two thirds of the number required for the oversized single mode aperture.

Figure 17 shows four H-plane power transmission factor curves for unloaded and dielectrically loaded apertures with and without the higher order LSE_{20} mode. The basic, unloaded H-plane pattern (dash-dotted) has two grating lobes at the -10.5 dB level for broadside radiation and one at the -8.5 dB level after scanning only to $(dx/\lambda) \sin \theta = 0.1$. Scan to $(dx/\lambda) \sin \theta = 0.3$ produces a grating lobe at about -5.5 dB. The introduction of a higher order (LSE_{20}) mode results in the dotted element pattern and, depending upon whether one uses the odd mode for broadside or introduces it after a degree of scan, one obtains a grating lobe of -5 to -6 dB at (q = 1). Nevertheless, this geometry offers extremely wide angle scanning to $(dy/\lambda) \sin \theta = 0.7$.

Use of dielectric layers to narrow the H-plane element pattern results in an LSE_{10} mode pattern as shown in the solid curve of Figure 17. This curve is drawn for a dielectric of thickness 0.2λ and constant 2.6. Without higher mode control, the array can evidently be scanned to approximately $(dy/\lambda) \sin \theta = 0.25$ for about a -9.0 dB grating lobe level and only 1 dB insertion loss.

The dashed curve of Figure 17 demonstrates the scanning characteristics of the loaded multimode H-plane horn and clearly indicates that the fall-off and grating lobe levels make multimode scanning in this plane far inferior to that in the E-plane (Figure 16 - dashed). Scan to $(dx/\lambda) \sin \theta = 0.6$ in both planes results in an element use factor of 2.78, but this is accomplished with over 3 dB loss at the maximum H-plane scan angle, and a grating lobe at approximately -8 dB.

Table 1 shows a comparison of the various options for H-plane pattern control along with the number of E-plane rows necessary to maintain -20 dB grating lobe suppression in the H-plane. In computing the grating lobe suppression by element displacement, one notes that the suppression value 6 dB was chosen for 8 rows, 10 dB for 16 rows and thereafter values 2 dB less than the maximum $10 \log N_y$ were used in order to provide a conservative estimate of the expected suppression. The element use factor has been computed in each case assuming E-plane scan with an LSE_{11} mode to $(dy/\lambda) \sin \theta = 0.6$. The term "normalized scan limit" is the $(dx/\lambda) \sin \theta_{max}$ divided by the required number of controls per element (2 - for odd mode).

The options defined by the table lead to two relatively clear choices, depending upon whether the array has enough rows to produce the required grating lobe suppression using row displacement. For a large array with more than 64 rows, the lowest element use factor is obtained with the unloaded aperture and using an odd H-plane distribution, as well as the odd E-plane distribution. This geometry has excellent gain fall-off in both planes, and an element use factor of only 2.4,

34

Table 1. H-Plane Design Data

		Normalized Scan Limit	El. Use Factor	Approximate Power Levels			Required N_y for -20 dB
				Broadside GL Level	End of Scan GL Level	End of Scan Gain	
1.	Unloaded H-Plane	0.3	2.77	-9.5	-5 dB	-1.6 dB	64
2.	Unloaded H-Plane with added LSE_{20} and LSE_{11}	0.35	2.4	-5 to -6	-7 dB	-1 dB	64
3.	Dielectric Loaded H-Plane	0.3	2.77	$-\infty$	-8 dB	-1.5 dB	25
4.	Dielectric Loaded H-Plane with added LSE_{20}	0.3	2.77	$-\infty$	-7 dB	-3 dB	25

which is more than competitive with most present array-reflector systems. The high H-plane grating lobes are suppressed by row displacement, but with 64 rows of large aperture elements, the array beamwidth must be extremely narrow (about one third of a degree for $dy/\lambda = 3$).

The logical choice for smaller arrays is the use of a dielectric loaded H-plane aperture with a single incident mode. Table 1 illustrates that there is little advantage to the use of any H-plane higher model control in this case, for the normalized scan limit and grating lobe levels are unchanged, but in order to maintain the same element use factor, the distribution with higher order mode control suffers an increased scan loss at the end of scan.

Figures 18 and 19 show the radiation characteristics of a uniformly illuminated 64-element array with $(dx/\lambda) = 3.37$ and $(dy/\lambda) = 4.5$ and designed to scan to 7.7^O in the E-plane and 10.26^O in the H-plane. The chosen example uses higher order mode control in both planes with dielectric loaded apertures for good performance at broadside. The dielectric slab thickness is 0.2λ which is slightly thicker than that used in the previous experiment. The dielectric constant is 2.6. The eight rows are displaced according to the values given in Eq. (25). This example does not correspond to one of the optimum choices above, but it does illustrate all of the various techniques used in this development. The figures show E-plane cuts through the main beam and all H-plane grating lobes, and thus record all undesired lobes at their maxima. The data shown include two cases corresponding to main beam locations at the maximum scan in the H-plane and the point of maximum E and H-plane scan in the intercardinal plane. Broadside data are not shown because for the chosen case all grating lobes are suppressed below -35 dB at broadside. The case of pure E-plane scan is not shown either, because
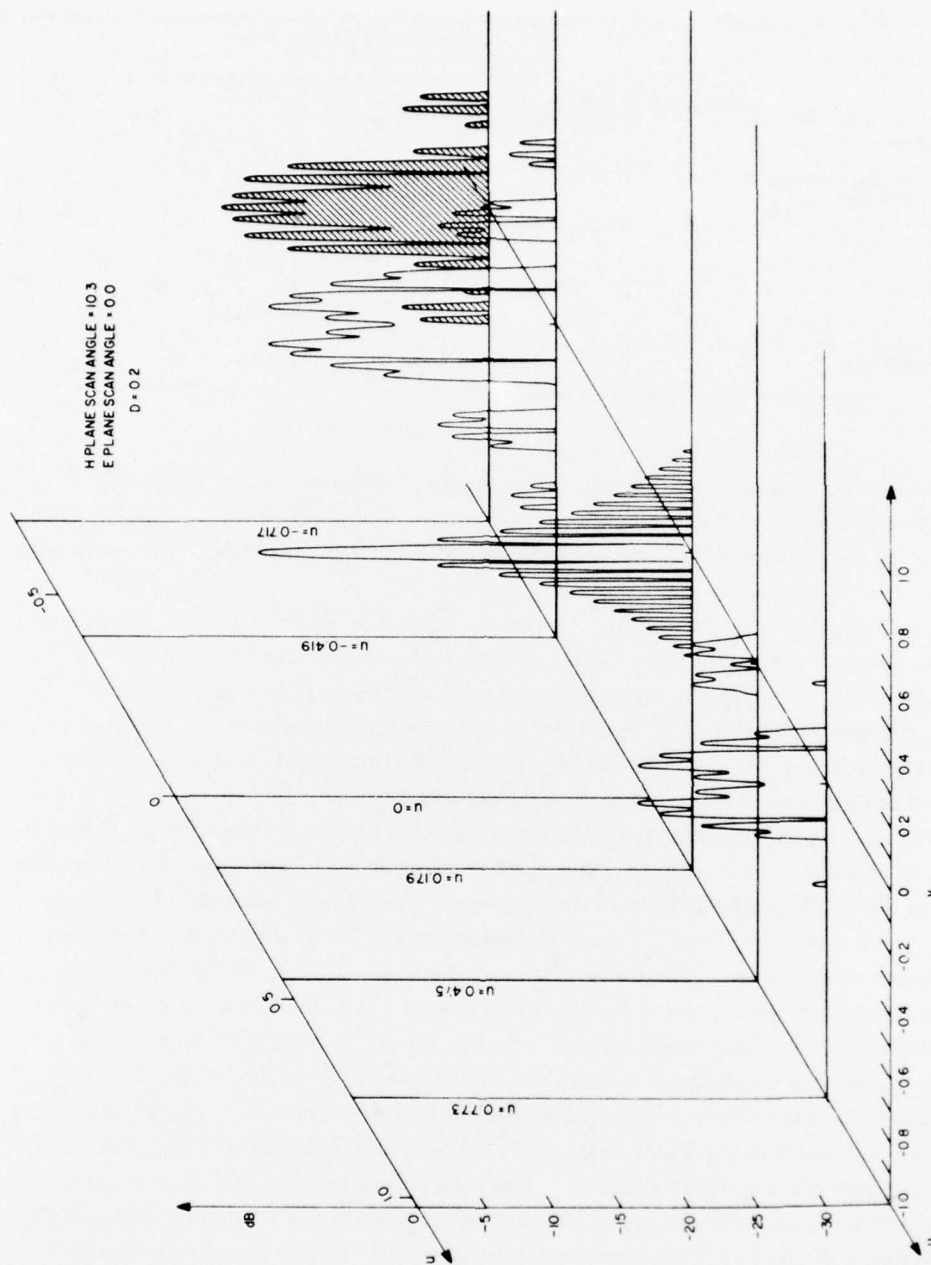
35

Figure 18. Grating Lobe Spectrum for 64-Element Array: Maximum E-Plane Scan
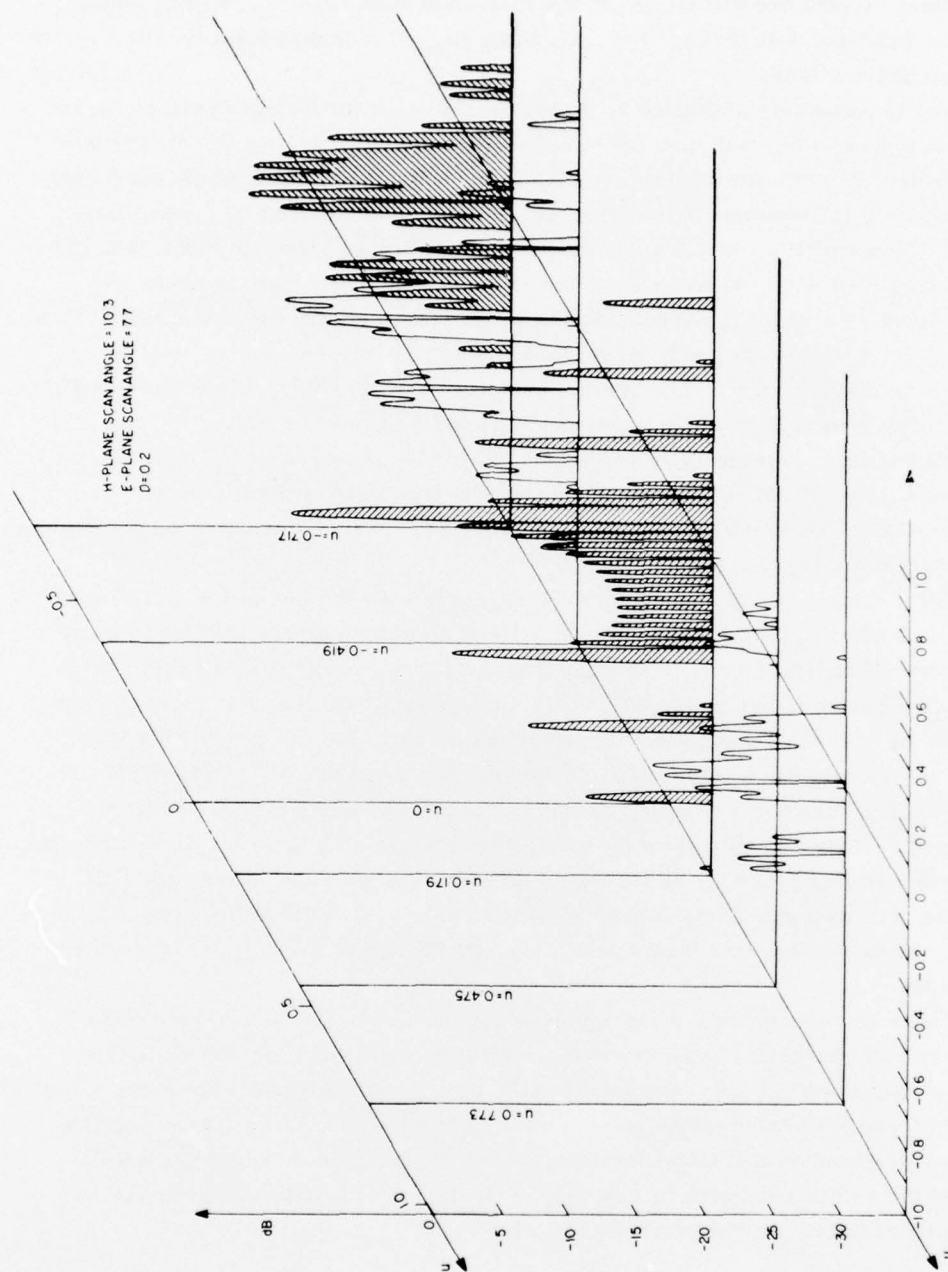
Figure 19. Grating Lobe Spectrum for 64-Element Array: Maximum Scan in both E- and H-Planes

37

for that case only the lobes for the u = 0 cut are at levels greater than -35 dB and these may be obtained directly from the maximum scan case (u_m, v_m) by adding 3 dB to the E-cut data through the main beam (u_m, v) to compensate for the H-plane element pattern loss.

The E-plane cuts of Figure 18 depict the situation for H-plane scan to 10.26° $(u_o = 0.178, v_o = 0)$, and show about 2.5 dB loss in main beam gain relative to broadside. The cut through the main beam $(u_o = 0.178, v)$ exhibits the characteristic pattern for uniform illumination with -13 dB sidelobes and no grating lobes. The E-plane cut (u_{-1}, v) has all lobes below -35 dB due to the odd mode, and the cut at $(u_{-2} = -0.4145, v)$ has a suppressed grating lobe structure at about the -12.5 level relative to the broadside beam; this grating lobe was computed at -7.5 without the row displacement, confirming the 6-7 dB suppression available with the chosen displacement. The grating lobe at $(u_{-3} = -0.7112, v)$ is at the -15 dB level. The grating lobe at $(u_1 = +0.4757, v)$ has a different distribution from the u_{-2} grating lobe, as noted also in Figure 18, and its peak reaches a level of approximately -29 dB relative to the broadside gain. The grating lobe at $(u_2 = 0.7725, v)$ are at about -21 dB and have, as expected, the same form as other even-order grating lobes (u_{-2}, v).

The E-plane cuts of Figure 19 show the radiation behavior at the end of scan $(u_{max} = 0.178, v_{max} = 0.133)$. These pattern distributions are similar to those of Figure 18 except for minor changes due to symmetry. The main beam gain is at -4 dB relative to broadside (3 dB loss for H-scan, 1 dB loss for E-scan), and the cut through (u_{max}, v) shows the usual -12 dB level for the v_{-1} grating lobe below the peak of the v_o main lobe. Other grating lobes are at the same relative levels as for pure E-plane scan, as this cut is totally unaltered by the row displacement. Other E-cuts show the suppression achieved by row displacement, and again the cut through (u_{-2}, v) shows the largest grating lobe at about -13.5 dB relative to broadside. This lobe is at approximately -7.5 dB without row displacement. Other grating lobe levels are below -20 dB except the (u_{-3}, v) lobe which is -16 dB.

These H-plane grating lobes are each suppressed by the amount predicted using row displacement and support the estimates of Table 1 for -20 dB levels. None of these calculations have included the use of spatial filters, however, which would be required for E-plane lobe correction in any case, and so for any given number of elements the actual H-plane grating lobes would be suppressed well beyond the values predicted by row displacement, or alternatively fewer rows would be required for any given suppression ratio.

38

6. CONCLUSION

This report has summarized the results of an extensive study undertaken to determine the potential and limitations of large array elements in a phased array with limited sector coverage. The primary subject of the report is a technique for using multiple higher order mode control at the apertures to suppress the grating lobes that arise when the array is scanned.

Since earlier reports have demonstrated the general scanning capability of the technique, the purpose of the report has been to analyze each of the problem areas of multiple mode limited scan systems, and to determine to the fullest degree possible whether these represented fundamental limitations or whether they could be overcome by design techniques. The cost of a full two-dimensional array test bed is prohibitive at this time and so the determination has been based on one-dimensional array data on theoretical calculations and on element patterns scanned in one or both planes.

The first area of investigation was the element pattern null filling due to phase distortion in the E-plane horns used in the previous experiments. This null filling raised the broadside grating lobes to about the -15 dB level, but experiments with dielectric lenses in an 8-element array showed that properly collimating the beam could reduce these levels to -18 to -20 dB without raising the cross polarized radiation beyond approximately -19 dB at the maximum scan "worst case" condition.

Other experiments have indicated that the effects of unwanted higher order modes can cause null filling and thus raise residual grating lobe levels to nearly the -16 dB level at frequencies that would otherwise be within the array design frequency band. With these contributions suppressed, the design bandwidth can exceed 10 percent.

Another factor that was investigated is the maximum grating lobe level of an array as a function of the number of array elements and the array amplitude taper (sidelobe level). These factors influence the grating lobe level because the width of the element pattern null is fixed, but the array beamwidth at the grating lobes varies with array size and taper. Thus for a very large array the entire beam can be placed at the deepest section of the element pattern null, but for smaller arrays or highly tapered arrays the null is too narrow to suppress the lobe completely. Data are given that show broadside and end-of-scan levels for a variety of Chebyshev distributions and array sizes and these data indicate that arrays with eight or more elements in the scan plane can have -20 dB sidelobe suppression with near sidelobes as low as -40 dB. The data also indicate that grating lobe levels below -25 dB can only be achieved with very large arrays.

Experimental and theoretical studies of H-plane and dual plane scan have shown that the use of dielectric slabs can narrow the H-plane pattern and thus reduce

39

the nearest H-plane grating lobes to zero for broadside radiation at the expense of higher second grating lobes ($p = \pm 2$) and increased loss at the higher scan angles. All of these data indicate that the pattern characteristics for H-plane scan are far inferior to the E-plane scan case, and that it is difficult to achieve much scan without excessive grating lobes in this plane.

Two techniques have been investigated for suppression of these far grating lobes. The simple displacement of adjacent rows or columns is shown to lead to suppression of selected grating lobes and to provide up to 10 log N dB of suppression for an array of N rows or columns. Selecting displacements which are symmetric about the array center allows grating lobe suppression without destroying monopulse nulls, and so is entirely consistent with radar applications. Finally, this approach does not destroy the array periodicity along any row or column that is displaced, and is thus still appropriate for row-column steering. The grating lobe suppression thus provided holds for all but those in the plane formed by the main beam and a perpendicular to the plane of the displacement, so that in Figure 18 the beams (u_o, v_q) are unchanged by displacement, but all others are suppressed. This leaves as remaining the principal plane grating lobes in the plane orthogonal to displacement, and thus primarily the E-plane lobes with their characteristic -12 dB lobe at $q = -2$.

The second technique investigated for far grating lobe suppression is the use of a spatial filter. Data are presented that demonstrate grating lobe suppression of this dominant $q = -2$ E-plane lobe for the 8-element limited scan array of Figure 7. Although spatial filtering is a frequency dependent technique, the Chebyshev design has the advantage that the spatial passband merely broadens and narrows as a function of frequency, and it is often possible to choose a design that is not adversely affected by frequency change.

The combination of these two approaches provides sufficient grating lobe suppression to guarantee -20 dB lobes (or lower) for all "far" grating lobes, and indeed for all grating lobes except those "near" lobes in the plane perpendicular to the displacement (in the example case $p = \pm 1$). As pointed out earlier, these lobes can approach -18 to -20 dB with proper design and are nearly always less than -16 dB, but they represent critical design areas which cannot be corrected by the displacement or filtering techniques.

A substantial effort has been devoted to outlining possible tradeoffs between the use of multiple modes for two-dimensional scan or for only a single plane. Results have indicated that two distinctly different solutions are to be preferred depending upon the array size, and that in fact for a very large array it is most appropriate to use a higher order mode in only one plane while relying on filters and element displacement to suppress grating lobes in the other plane. Details of those and other tradeoffs are described in detail to enable the designer to make appropriate choices of dimensions and array techniques.

40

References

1. Patton, W. T. (1972) Limited scan arrays, in Phased Array Antennas, Proc. 1970 Phased Array Antenna Symposium, A. A. Oliner and G. H. Knittel, Ed., Artech House, Inc., Dedham, Mass., pp. 332-343.

2. Tang, R. (1972) Survey of time-delay beam steering techniques, in Phased Array Antennas, Proc. 1970 Phased Array Antenna Symposium, Artech House, Inc., Dedham, Mass., pp. 254-260.

3. Mailloux, R. J. and Blacksmith, P. (1974) Array and reflector techniques for airport precision approach radars, Microwave Journal, pp. 35-38.

4. Howell, J. M. (1974) Limited scan antennas, IEEE Trans. APS International Symposium.

5. Mailloux, R. J. (1974) An overlapped subarray for limited scan application, IEEE Trans AP AP-22:487-489.

6. Stangel, J., and Ponturieri, J. (1972) Random subarray techniques in electronic scan antenna design, IEEE G-AP International Symposium.

7. Mailloux, R. J., and Forbes, G. R. (1973) An array technique with grating-lobe suppression for limited-scan application, IEEE Trans. AP AP-21 (No. 5):597-602.

8. Manwarren, T. A., and Minuti, A. H. (1974) Zoom Feed Technique Study, RADC-TR-74-56, Final Technical Report.

9. Stangel, J. J. (1974) A basic theorem concerning the electronic scanning capabilities of antennas. Paper presented at URSI Commission VI spring meeting.

10. Borgiotti, G. V. (1975) Degrees of freedom of an antenna scanned in a limited sector, IEEE Trans AP-S International Symposium.

11. Zahn, L. (1974) Design of a Collimating Lens for a Limited Scan Array, AFCRL-TR-74-0492, Physical Sciences Research Papers, No. 223.

12. Mailloux, R. J., and Forbes, G. R. (1973) Experimental Studies of a Multiple Mode Array Technique for Limited Scan Application, AFCRL-TR-73-0685, Physical Sciences Research Papers, No. 575.

41

13. Tsandoulas, G. N., and Fitzgerald, W. D. (1972) Aperture efficiency enhancement in dielectrically loaded horns, IEEE Trans. AP AP-20 (No. 1): 69-74.

14. Mailloux, R. J. (1976) Synthesis of spatial filters with Chebyshev Characteristics, IEEE Trans. AP AP-24(No. 2):174-181.

Appendix

Bandwidth of Spatial Filters with Chebyshev Characteristics

Spatial filters designed according to the analytical treatment of Reference 14 have limited frequency bandwidth because their characteristics are Chebyshev in frequency as well as angle.

The power loss polynomial used throughout that analysis is

$$A_{11} A_{11}^* = 1 + \Delta^2 T_m^2 (\sin \zeta / \sin \zeta_1) \tag{A1}$$

where

$$\zeta = \frac{2\pi S}{\lambda} \cos \theta = \frac{2\pi f}{c} S \cos \theta \tag{A2}$$

and ζ , is the value of ζ at the passband edge, S is the interlayer spacing, f and λ the frequency and wavelength, and C the velocity of light.

An advantage of the Chebyshev design is that the spatial characteristics merely narrow and broaden as a function of frequency, and this need not seriously alter filter effectiveness provided that there is adequate separation between the maximum passband angle and the nearest grating lobe or sidelobe requiring rejection.

Figure A1 shows a typical spatial coverage as a function of frequency, and indicates that the passband is narrowest at the lowest frequency f_{-1} and broadest at the high frequency f_1. An estimate of filter bandwidth is obtained as follows:

43

At f_{-1}, set $\sin \zeta$ equal to $K_1 \sin \zeta_1$ at the maximum passband angle. This allows θ_m to occur in a region where there may be some tolerable rejection. The value of K_1 is selected as unity or some larger value as associated with the tolerable rejection ratio.

$$\zeta_m = \frac{2\pi f_{-1}}{c} S \cos \theta_m = \frac{2\pi S}{\lambda_{-1}} \cos \theta_m \text{ and } \sin \zeta_m = K_1 \sin \zeta_1 \tag{A3}$$

or approximately:

$$(n\pi - \zeta_m) = K_1 (n\pi - \zeta_1) . \tag{A4}$$

Here $n\pi$ has been subtracted from ζ_1 to allow the linearization. The integer n is unity for S/λ_{-1} approximately $1/2$, two for S/λ_{-1} approximately unity, and so on. The condition above also serves to define the interlayer spacing using:

$$\frac{S}{\lambda_{-1}} = \frac{1}{2\pi \cos \theta_m} \left[n\pi - K_1 (n\pi - \zeta_1) \right] \tag{A5}$$

$$= \frac{1}{2\pi \cos \theta_m} \left[n\pi - K_1 \overline{\zeta}_1 \right] , \text{ which defines the variable } \overline{\zeta}.$$

At the high frequency f_1, set $\sin \zeta$ equal to $K_2 \sin \zeta_1$ at the grating lobe angle θ_{g1}. Here K_2 is chosen to provide the desired suppression at the grating lobe. Again linearizing the expression after subtracting $n\pi$ leads to:

$$n\pi - \zeta_{g1} = K_2 (n\pi - \zeta_1) . \tag{A6}$$

Combining this with Eq. (A4) one gets

$$n\pi - \frac{2\pi f_1}{c} S \cos \theta_{g1} = \frac{K_2}{K_1} \left(n\pi - \frac{2\pi f_{-1}}{c} S \cos \theta_m \right).$$

Setting $f_1 = f_{-1} + \delta$, one obtains an expression for percentage bandwidth, relative to the low frequency f_{-1}.

$$\frac{\delta}{f_{-1}} = -\frac{1}{2} \left(\frac{\lambda_{-1}}{S} \right) \frac{1}{\cos \theta_{g1}} (n) \left(\frac{K_2}{K_1} - 1 \right) - \left(1 - \frac{K_2}{K_1} \frac{\cos \theta_m}{\cos \theta_{g1}} \right) . \tag{A7}$$

44

This expression, used with Eq. (A5), provides a solution for bandwidth based upon the condition that there be sufficient grating lobe rejection at the high frequency.

In certain cases the bandwidth may be restricted further by the condition that at the high frequency the broadside angle ($\theta = 0$) will suffer some rejection. This is so if

$$\left| \sin \zeta \right| = \left| \sin \left(2 \pi f_1 \frac{S}{\lambda} \right) \right| \geq \left| \sin \zeta_1 \right| . \tag{A8}$$

When this occurs, this relationship, rather than Eq. (A6) determines the bandwidth. This does not occur for the filter described in the report, and so it is recorded here for completeness.

Equation (A7) may be combined with an approximate form of Eq. (A5) to give a particularly convenient form for cases in which $K_1 \bar{\zeta}$ is small compared to $n\pi$. In this case the resulting approximation is:

$$\frac{\delta}{f_{-1}} = -1 + \frac{\cos \theta_m}{\cos \theta_{g1}} \left[1 - \left(\frac{K_2}{K_1} - 1 \right) \frac{K_1 \bar{\zeta}}{n\pi} \right] . \tag{A9}$$

An example of the use of these formulae for the filter shown in this report follows.

Consider that the array scans to 10.25^O and a grating lobe comes within 24.7^O of broadside. Using $\sin \zeta_1 = 0.15$, $\cos \theta_m = 0.984$, $\cos \theta_{g1} = 0.909$, and setting $K_1 = 1.85$ for about 0.6 dB rejection at the θ_m for the lowest frequency and $K_2 = 2.94$ for about 6.5 dB grating lobe rejection at the highest frequency, one obtains $S/\lambda_{-1} = 0.97$ (n = 2) and the bandwidth is computed to be 5.2 percent using Eq. (A7) and (A5) or 5.4 percent using Eq. (A9).

Equation (A9) also gives the bandwidth for the ideal Chebyshev-type filter, for if the rejection slope could be infinitely steep, then K_2/K_1 could be unity and still provide perfect rejection; and in that case

$$\frac{\delta}{f_{-1}} = \frac{\cos \theta_m}{\cos \theta_{g1}} - 1 . \tag{A10}$$

45

MISSION
of
Rome Air Development Center

RADC plans and conducts research, exploratory and advanced development programs in command, control, and communications (C^3) activities, and in the C^3 areas of information sciences and intelligence. The principal technical mission areas are communications, electromagnetic guidance and control, surveillance of ground and aerospace objects, intelligence data collection and handling, information system technology, ionospheric propagation, solid state sciences, microwave physics and electronic reliability, maintainability and compatibility.